Available online at www.sciencedirect.com

SciVerse ScienceDirect

Scripta Materialia 66 (2012) 992–996

Scripta MATERIALIA

www.elsevier.com/locate/scriptamat

Viewpoint Paper

Grain size effect on strain hardening in twinning-induced plasticity steels

I. Gutierrez-Urrutia* and D. Raabe

Max-Planck-Institut für Eisenforschung, Max-Planck Str. 1, D-40237 Düsseldorf, Germany

Available online 28 January 2012

Abstract—We investigate the influence of grain size on the strain hardening of two Fe–22Mn–0.6C (wt.%) twinning-induced plasticity steels with average grain sizes of 3 and 50 μm, respectively. The grain size has a significant influence on the strain hardening through the underlying microstructure. The dislocation substructure formed in the early deformation stages determines the density of nucleation sites for twins per unit grain boundary area which controls the developing twin substructure.

Keywords: TWIP steels; Plastic deformation; Dislocation structure; Twinning; Scanning electron microscopy (SEM)

TWIP (twinning-induced plasticity) steels have been the object of much interest in recent years due to their outstanding mechanical properties at room temperature combining high strength (ultimate tensile strength up to 800 MPa) and ductility (elongation to failure up to 100%) based on a high work-hardening capacity [1–5]. TWIP steels are typically austenitic steels, i.e. face-centered cubic (fcc) alloys, with a high Mn content (above 20 wt.%) and additions of elements such as carbon (<1 wt.%), silicon (<3 wt.%) or aluminum (<10 wt.%). The TWIP mechanism is observed in medium stacking fault energy steels (20–40 mJ m^{-2}) and is characterized by the formation of nanometer-thick deformation twins. The strain hardening is commonly analyzed in terms of the dislocation mean free path (MFP) approach, focusing essentially on a single microstructure parameter, namely the twin spacing [3,6,7]. These works attribute the high strain-hardening rate at intermediate strains (0.1–0.2 true strain) to twin spacing refinement. As twin boundaries are major obstacles to dislocation glide, the increasing density of deformation twin boundaries with further deformation leads to the so-called "dynamic Hall–Petch effect". However, as we have recently shown in Ref. [4], this concept conveys an overly simplistic picture of the strain-hardening behavior. High-manganese TWIP steels are characterized by a hierarchical microstructure refinement involving different dislocation substructure sizes and twin spacings, which are determined by the stress level. At the early stages of deformation (below 0.1 true strain), the microstructure consists of dislocation cells and cell blocks containing highly dense dislocation walls. These dislocation substructures are major barriers to dislocation glide resulting in an early high strain hardening. At intermediate strains (0.1–0.3 true strain), a well-defined twin substructure is developed. As twinning depends strongly on the crystallographic grain orientation, the resulting deformed microstructure is a complex mixture of dislocation and twin substructures. At this strain level, different microstructure parameters control strain hardening, such as the average dislocation cell size and twin spacing.

However, it is not only crystallographic orientation that has a strong influence on deformation twinning; grain size also plays a part. Only a few studies have addressed the influence of grain size on deformation twinning in TWIP steels [8–10]. For instance, we recently observed [9] that the influence of grain size on the twinning stress within the micrometer grain size range in a Fe–22Mn–0.6C (wt.%) TWIP steel can be explained in terms of a Hall–Petch relation. It is thus clear that there are still some details that remain unclear regarding the influence of grain size on the strain-hardening behavior in TWIP steels, in particular its role on the twin substructure. The present study aims at elucidating the influence of grain size on the strain-hardening behavior of a Fe–22Mn–0.6C TWIP steel. We analyze the role of grain size on the corresponding dislocation and twin substructures. Detailed microstructural observations by electron channeling contrast imaging (ECCI) were performed on two

* Corresponding author. Tel.: +49 2116792 407; e-mail: i.gutierrez@mpie.de

1359-6462/$ - see front matter © 2012 Acta Materialia Inc. Published by Elsevier Ltd. All rights reserved.
doi:10.1016/j.scriptamat.2012.01.037

types of tensile samples deformed to different strain levels at room temperature. The specimens had average grain sizes of 3 and 50 μm, respectively.

The TWIP steels used in this study had the chemical composition Fe–22Mn–0.6C (wt.%). The material was melted in an induction furnace under Ar atmosphere and cast into round bars of 25 mm in diameter. Samples were swaged to 20% area reduction at 1000 °C and subsequently solution treated for 4 h at 1100 °C under Ar. Thereafter, samples were hot-rolled to 75% thickness reduction at 1000 °C, followed by air cooling. To obtain samples with different grain sizes, the hot-rolled steel was then cold rolled to 70% thickness reduction and annealed at 700 °C for different times. We obtained fully recrystallized steels with average grain sizes of 3 μm (referred to as FG-steel) and 50 μm (referred to as LG-steel) after annealing times of 5 and 15 min, respectively. The steels showed a fully austenitic structure which remained stable during deformation at room temperature. No evidence of ε-martensite was detected by electron back-scatter diffraction (EBSD) on the tensile deformed samples. Tensile tests were performed at room temperature at an initial strain rate of $10^{-4}\,s^{-1}$ to different strain levels. The mechanical tests were carried out on a tensile test instrument (Kammrath & Weiss GmbH, Dortmund, Germany) equipped with a digital image correlation (DIC) system (ARAMIS system, GOM-Gesellschaft für Optische Messtechnik mbH, Braunschweig, Germany) to measure the local and macroscopic strain distribution. Details of this set-up are described in Ref. [11]. The surface pattern required for DIC was obtained as explained in Ref. [9]. Averaged engineering strain values were retrieved from the corresponding strain maps and used to calculate the true stress–strain values. Dislocation and twin substructures were characterized by ECCI after orienting the crystal into the Bragg condition using a high-intensity reflection. We used a new recently reported EBSD-based ECCI set-up [12] that allows ECCI images to be obtained under controlled diffraction conditions with enhanced dislocation contrast. This ECCI set-up has been successfully used in the imaging and quantification of dislocation substructures in Fe-based alloys [4,9,13]. ECCI observations were carried out in a dual-beam Zeiss-Crossbeam instrument (Carl Zeiss SMT AG, Germany) consisting of a Gemini-type field emission gun (FEG) electron column and a focused ion beam device (Orsay Physics FIB). This instrument is equipped with an EBSD system (EDAX/TSL, Draper, UT, USA). ECCI was performed at 10 kV acceleration voltage and a working distance of 6 mm, using a solid-state four-quadrant BSE detector.

Figure 1a shows the true stress–strain curves of the Fe–22Mn–0.6C (wt.%) TWIP steels with average grain sizes of 50 μm (LG-steel) and 3 μm (FG-steel) tensile deformed at an initial strain rate of $10^{-4}\,s^{-1}$. Figure 1a shows that the grain size has a significant influence on the yield stress. This can be explained by the Hall–Petch relation: $\sigma_y = \sigma_0 + K_{tw}^{H-P}/\sqrt{D}$, where σ_y is the yield stress, σ_0 is the friction stress, K_{tw}^{H-P} is a constant, and D is the initial grain size. Using appropriate values of the constants [9], we obtain yield stresses of 207 and 360 MPa for the LG-steel and FG-steel, respectively. These stresses are close to the experimental values of 210 and 330 MPa.

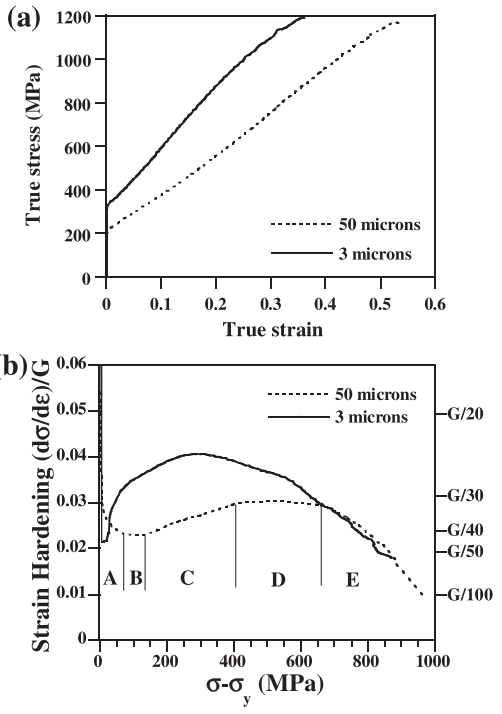

Figure 1. (a) True stress–true strain curves of the Fe–22Mn–0.6C (wt.%) TWIP steels with average grain sizes of 50 μm (referred to as LG-steel) and 3 μm (referred to as FG-steel) tensile deformed at an initial strain rate of $10^{-4}\,s^{-1}$. (b) Normalized strain-hardening rate (normalized by the shear modulus) vs. flow stress subtracted by the yield stress of the tensile deformed TWIP steels.

Figure 1b shows the normalized strain-hardening rate (normalized by the shear modulus) vs. flow stress subtracted by the yield stress, $\sigma - \sigma_y$, of the tensile deformed TWIP steels. The strain hardening of the LG-steel has been analyzed in detail in Ref. [4], and accordingly only the main aspects will be discussed here. The LG-steel exhibits five different deformation stages. The first stage, stage A hardening, is characterized by a continuous decrease in the strain-hardening rate. This stage is ascribed to the prevalence of dynamic recovery processes such as cross-slip and annihilation of screw dislocations of opposite signs. The second stage, Stage B hardening, which is characterized by a constant strain-hardening rate with a hardening coefficient of about G/40 (where G is the shear modulus), is attributed to dislocation substructure hardening. The development of a dense twin substructure upon straining results in a further drastic refinement of the dislocation mean free path (MFP). Consequently, strain hardening increases up to a hardening coefficient of about G/30, stage C hardening. With further straining, the reduced additional refinement of the dislocation and twin substructures, together with the increasing strengthening effect of the individual deformation twins as obstacles to dislocation glide, reduce the capability for trapping more dislocations and, hence, the strain hardening decreases (stages D and E). It is interesting to note that the onset of the high strain-hardening stage of the FG-steel occurs at a value of σ-σ_y of 20 MPa, which is roughly 120 MPa smaller than the onset of stage C hardening of the LG-steel. As the

yield stress, σ_y, of the FG-steel is about 120 MPa higher than that of the LG-steel, this indicates that both hardening stages occur at the same macroscopic stress level. ECCI images of deformed microstructure of the FG-steel deformed to strain/stress levels ranged between 0.03 true strain/390 MPa and 0.2 true strain/860 MPa (Fig. 2b and c), confirm that the high strain-hardening rate of the FG-steel is due to microstructure refinement by deformation twinning. According to the previous classification of hardening stages in TWIP steels, the FG-steel exhibits only four different deformation stages, namely stages A, C, D and E. It is interesting to note the main features revealed in the strain-hardening curves of the TWIP steels (Fig. 1b). These are, first, the rapid increase in strain hardening in the FG-steel immediately after yielding, i.e. the absence of stage B hardening; and second, the significantly higher stage C hardening of the FG-steel (strain-hardening coefficient of about G/25). The absence of stage B hardening in the FG-steel implies that the refinement of the mean free path by deformation twinning occurs at a strain level just slightly higher than the onset of yielding. However, the higher strain hardening associated with deformation twinning observed in the FG-steel, i.e. stage C hardening, deserves more detailed analysis of the underlying deformation microstructure.

The ECCI image of Figure 2a shows the deformed microstructure of the FG-steel strained to 0.03 true strain, stage C hardening. Under the current diffraction conditions, the crystal matrix appears dark and dislocations appear as sharp bright lines due to the electron channeling mechanism [14]. Figure 2a reveals that the deformed microstructure consists of loose dislocation arrangements. This dislocation substructure is very different from that observed in the LG-steel at the onset of stage C hardening (Fig. 3a and b). These figures show ECCI images of the dislocation substructure at 0.1 true strain in cross section. Figure 3a and b correspond to crystals oriented close to the ⟨0 0 1⟩//tensile axis and ⟨1 1 2⟩//tensile axis, respectively. Figure 3a shows that

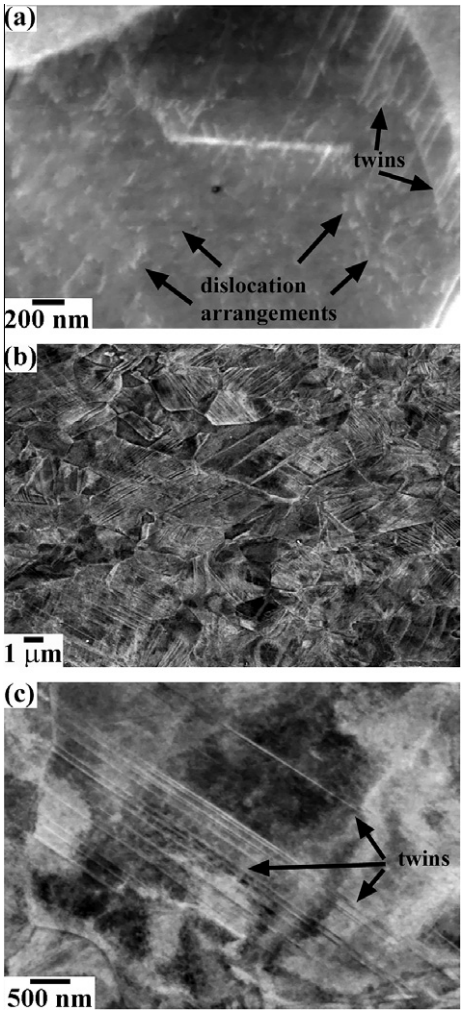

Figure 2. ECCI images of deformed microstructure of the FG-steel. (a) Loose dislocation arrangements and deformation twins nucleated at grain boundaries on a sample tensile deformed to 0.03 true strain. Corresponding features are indicated by arrows. (b) Twin substructure of a sample tensile deformed to 0.2 true strain. (c) Detail of lamellar twin structure in a sample deformed at a true strain of 0.2.

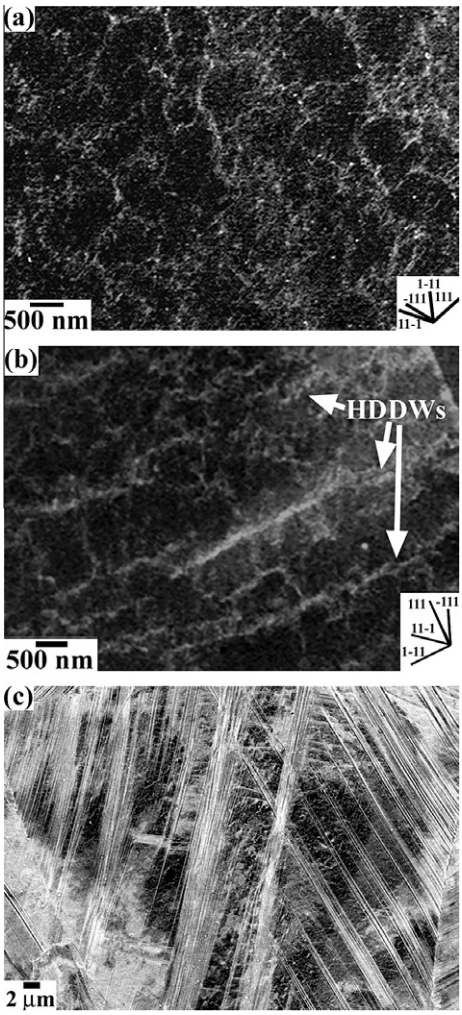

Figure 3. ECCI images of deformed microstructure of the LG-steel. (a) Dislocation cells (DCs) in a sample deformed at a true strain of 0.1, cross-section view. (b) Cell-block structure delimited by highly dense dislocation walls (HDDWs) in a sample deformed at a true strain of 0.1, cross-section view. Corresponding features are indicated by arrows. (c) Detail of multiple twin structure in a sample deformed at a true strain of 0.3.

the dislocation substructure of the first crystal consists of equiaxed dislocation cells (DCs). These structures appear under the current Bragg condition using a high-intensity reflection of {1 1 1}-type as bright globular structures with a sharp boundary contrast. The second crystal contains cell blocks mainly delimited by highly dense dislocation walls (HDDWs). These boundaries appear as straight and extended bright compact layers (indicated by arrows in the figure). This morphology corresponds to planar dislocation substructures commonly found in low-to-medium stacking fault energy metals [15,16]. In this case, only one set of HDDWs is observed. The dislocation patterns shown in Figure 3a and b are similar to those observed by bright-field TEM in medium-to-high stacking fault energy alloys [15–17]. However, the contrast in ECCI imaging is inverted compared to that obtained in bright-field TEM due to the electron channeling mechanism and the diffraction conditions used to image dislocation substructures. These dislocation substructures are ascribed to the multiple character of slip, namely wavy and planar. Wavy dislocation structures are promoted in grains when a high number of slip planes are activated and dislocation cross-slip is enabled [17]. Planar dislocation substructures in the present TWIP steel are associated with the high friction stress (157 MPa [7], which is higher than for materials exhibiting planar slip such as stainless steels [18]), and low stacking fault energy (22 mJ m^{-2} [19]).

ECCI images further reveal that TWIP steels develop different twin substructures in the C strain-hardening regime (Fig. 1). At 0.2-0.3 true strain, the twin substructure of the FG-steel is formed roughly equally by twin substructures containing either one or two active twin systems (determined from ECCI images of about 200 grains) (Fig. 2b). Figure 2c shows an example of lamellar twin structure in the FG-steel at a true strain of 0.2. However, at the same strain level, the twin substructure of the LG-steel mainly consists of two active twin systems [4] (two twin systems: 60% grain area fraction, one twin system: 30% grain area fraction, no twins: 10% grain area fraction). Figure 3c shows an example of multiple twin structure in the LG-steel at a true strain of 0.3.

These observations suggest that grain size has a significant influence on the deformed microstructure over the entire deformation range. The influence of grain size on the dislocation substructure formed at the early deformation stage, stage B hardening, can be understood in terms of the Hall–Petch relation. Due to the low yield stress, the LG-steel requires a larger strain to achieve the macroscopic stress associated to stage C hardening (0.1 true plastic strain). At this deformation stage, dislocation glide mainly controls plasticity and, accordingly, the dislocation density scales with strain. The high dislocation density in the LG-steel is mainly accumulated in the form of DCs and cell blocks delimited by HDDWs (Fig. 3a and b). However, due to the higher yield stress, the FG-steel stores a lower dislocation density before the onset of stage C hardening. The dislocation density in this deformation regime is accumulated in the form of loose dislocation arrangements (Fig. 2a).

The influence of grain size on the twin substructure is depicted in Figure 4. It can be rationalized as follows. First, the dislocation substructure formed during the early deformation stages (Fig. 4a and b) determines the density of nucleation sites for twins per unit grain boundary area. Second, the nucleation site density accounts for the evolving twin substructure (Fig. 4c and d). Deformation twinning can be considered as a nucleation and growth process [20]. Nucleation of deformation twins proceeds by specific dislocation reactions which are required for twin growth. There are several proposed dislocation reaction mechanisms in the literature. Basically, they can be divided into two groups: mechanisms which suggest a direct dislocation dissociation process under the action of a certain stress (pole mechanism [21]); and those mechanisms involving specific dislocation interactions with Lomer–Cottrell locks (perfect dislocations [22,23] or pile-ups of extended dislocations [24]). In particular, recent TEM observations in high-Mn steels [25,26] support those models involving dislocation interactions with Lomer–Cotrell locks. We further assume that grain boundaries are the main sites of twin nucleation in the present TWIP steels. High-resolution ECCI reveals that other intragranular interfaces, such as twin boundaries, act as twin nucleation sites only at high macroscopic stress levels. If we consider that twin nucleation is controlled by specific dislocation reactions, the rather homogeneous dislocation distribution of the FG-steel (Fig. 4a) provides a high number of nucleation sites for twins per unit grain boundary. On the other hand, the LG-steel contains a high overall dislocation density mainly distributed along the boundaries of the dislocation substructure, namely dislocation cell walls and HDDWs. As cell-forming crystals do not twin upon deformation [4], we only consider those crystals containing cell block structures mainly delimited by HDDWs (Fig. 4b). This dislocation substructure creates a lower number of nucleation sites

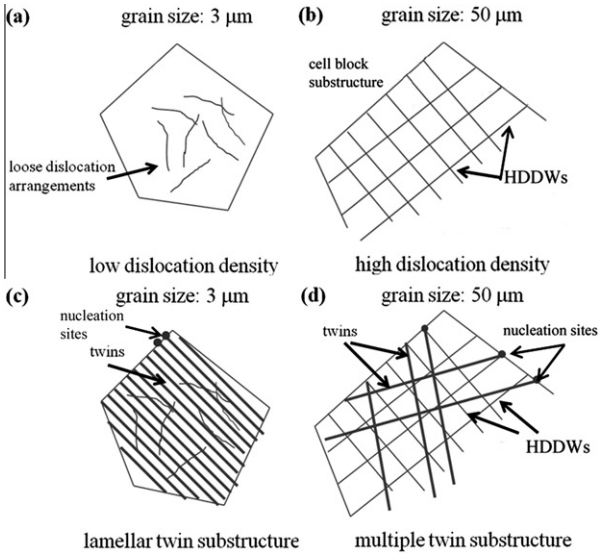

Figure 4. Schematic illustration of the influence of grain size on twin substructure in TWIP steels. (a, b) Effect of grain size on the dislocation substructure formed at the early deformation stages. (c, d) Effect of dislocation substructure on the density of nucleation sites for twins per unit grain boundary area, which controls the developing twin substructure. HDDWs, highly dense dislocation walls.

for twins per unit grain boundary. In other words, grain size has a negative effect on the number of twins per unit grain boundary area. This agrees with recent observations on Mg and Ti [27]. However, if we consider that the grain boundary area per unit volume is equal to 2/D (where D is the grain size), and assuming that twins are spheroids, Ghaderi and Barnett [27] have shown that a higher density of twin nucleation events per unit grain boundary area does not result in a higher twin volume fraction due to twin size effects (twin length and thickness are grain size dependent).

Twin growth proceeds by co-operative movement of Shockley partials on subsequent {1 1 1} planes, i.e. it is a stress-controlled process. A high density of twins per unit grain boundary area promotes the formation of a lamellar twin structure. This is due to the high local stress that would be required to push a second twin system through the existing lamellar twin structure containing an already high density of twin boundaries. If we consider here the crystallographic grain orientation, this effect is expected to be more relevant in crystal orientations where the Schmid factors for twinning on the two most favorable systems are similar. This means that lamellar twin structure is enabled in the FG-steel (Fig. 4c). On the other hand, a low density of twins per unit grain boundary area enables the formation of multiple twin structures due to the lower number of twin–twin interactions. Accordingly, a multiple twin structure is enhanced in the LG-steel (Fig. 4d). As we have shown in Ref. [4], the mean free path refinement by deformation twinning is responsible for the high strain hardening of TWIP steels. In particular, the formation of a lamellar twin structure is the most effective way to increase the strain hardening due to the small twin spacing. As a lamellar twin structure is promoted particularly in the FG-steel, the strain-hardening level in this material increases as well, as Figure 1b shows.

In summary, we have investigated the effect of grain size on the strain-hardening behavior in two Fe–22Mn–0.6C (wt.%) TWIP steels with average grain sizes of 3 μm (FG-steel) and 50 μm (LG-steel) by ECCI. We observe a strong influence of grain size on the strain-hardening behavior. This is ascribed to the microstructure formed upon straining, namely the dislocation substructure formed in the early deformation stages and the evolving twin substructure. The early dislocation substructure determines the density of nucleation sites for twins per unit grain boundary area, which controls the developing twin substructure.

Acknowledgments

The authors would like to acknowledge the financial support by the German Research Foundation in the framework of SFB 761 “steel ab initio”.

References

[1] O. Grässel, L. Krüger, G. Frommeyer, L.W. Meyer, Int. J. Plast. 16 (2000) 1391.
[2] S. Curtze, V.T. Kuokkala, Acta Mater. 58 (2010) 5129.
[3] O. Bouaziz, S. Allain, C.P. Scott, P. Cugy, D. Barbier, Curr. Opin. Solid State Mater. Sci. 15 (2011) 141.
[4] I. Gutierrez-Urrutia, D. Raabe, Acta Mater. 59 (2011) 6449.
[5] S.J. Lee, J. Kim, S.N. Kane, B.C. De Cooman, Acta Mater. 59 (2011) 6809.
[6] M.N. Shiekhelsouk, V. Favier, K. Inal, M. Cherkaoui, Int. J. Plast. 25 (2009) 105.
[7] J. Gil Sevillano, Scripta Mater. 60 (2009) 336.
[8] R. Ueji, N. Tsuchida, D. Terada, N. Tsuji, Y. Tanaka, A. Takemura, K. Kunishige, Scripta Mater. 59 (2008) 963.
[9] I. Gutierrez-Urrutia, S. Zaefferer, D. Raabe, Mater. Sci. Eng. A 527 (2010) 3552.
[10] G. Dini, A. Najafizadeh, R. Ueji, S.M. Monir-Vaghefi, Mater. Des. 31 (2010) 3395.
[11] D. Raabe, M. Sachtleber, Z. Zhao, F. Roters, S. Zaefferer, Acta Mater. 49 (2001) 3433.
[12] I. Gutierrez-Urrutia, S. Zaefferer, D. Raabe, Scripta Mater. 61 (2009) 737.
[13] I. Gutierrez-Urrutia, D. Raabe, Scripta Mater. (2012), doi:10.1016/j.scriptamat. 2011.11.027.
[14] A.J. Wilkinson, P.B. Hirsch, Micron 28 (1997) 279.
[15] X. Huang, Scripta Mater. 38 (1998) 1697.
[16] D. Canadinc, H. Sehitoglu, H.J. Maier, Y.I. Chumlyakov, Acta Mater. 53 (2005) 1831.
[17] B. Bay, N. Hansen, D.A. Hughes, D. Kuhlmann-Wilsdorf, Acta Metall. Mater. 40 (1992) 205.
[18] K.H. Lo, C.H. Shek, J.K.L. Lai, Mater. Sci. Eng. R 65 (2009) 39.
[19] L. Bracke, L. Kestens, J. Penning, Scripta Mater. 61 (2009) 220.
[20] J.W. Christian, S. Mahajan, Prog. Mater. Sci. 39 (1995) 1.
[21] J.A. Venables, Philos. Mag. 6 (1961) 379.
[22] S. Mahajan, G.Y. Chin, Acta Metall. 21 (1973) 1353.
[23] J.B. Cohen, J. Weertman, Acta Metall. 11 (1963) 996.
[24] S. Miura, J. Takamura, N. Narita, Trans. Jpn. Inst. Met. 9 (1968) 555.
[25] I. Karaman, H. Sehitoglu, K. Gall, Y.I. Chumlyakov, H.J. Maier, Acta Mater. 48 (2000) 1345.
[26] H. Idrissi, K. Renard, L. Ryelandt, D. Schryvers, P.J. Jacques, Acta Mater. 58 (2010) 2464.
[27] A. Ghaderi, M.R. Barnett, Acta Mater. 59 (2011) 7824.